MULTISCALE AND TURBULENT INTERACTIONS FOR URBAN MICROCLIMATE PREDICTION

A dissertation submitted to
ETH ZURICH

for the degree of
DOCTOR OF SCIENCES

presented by
MARCEL VONLANTHEN
Master of Science in Mechanical Engineering (EPF Lausanne)
born 15 September 1982
citizen of Lausanne, Switzerland

accepted on the recommendation of
Prof. Dr. Jan Carmeliet, examiner
Dr. Jonas Allegrini, co-examiner
Prof. Dr. Johan Meyers, co-examiner
Prof. Dr. Catherine Gorlé, co-examiner

2015

ABSTRACT

ZUSAMMENFASSUNG

ACKNOWLEDGMENTS

—

CONTENTS

1

INTRODUCTION

1.1 HOW TO CITE A PAPER

my introduction, I want to cite (Moeng et al., 2007) because he is cool, and also Pope (2000) even cooler. Yeah! The following commands give:

- cite: Moeng et al., 2007

- citep: (Moeng et al., 2007)

- citet: Moeng et al. (2007)

- textcite: Moeng et al. (2007)

See http://merkel.zoneo.net/Latex/natbib.php for more styles.

1.2 HOW TO MAKE INDEX

Direct Numerical Simulation (DNS) resolves all the scales of the problem. As it is an important topic, I have added DNS to the index. Large Eddy Simulation (LES) is also in the index. How to build the index:

1. Build the document with PDFLatex

2. Build the index with makeIndex

3. Build the document again with PDFLatex

Most of the latex editor have a buttom/shortcut for makeIndex. See http://en.wikibooks.org/wiki/LaTeX/Indexing for more information in indexing.

BACKGROUND

2.1 THE NAVIER-STOKES EQUATIONS

The microclimate over urban areas involves a wide range of flow scales. On the one hand, obstacles such as buildings, civil engineering structures or small terrain features, affect the atmospheric boundary layer. The topology of such obstacles results into small flow structures with a typical size of $\mathcal{O} = 10^0 m$. On the other hand, large scale effects, such as regional winds and convective cells, generate large scale eddies with a size of $\mathcal{O} = 10^2 m$. Resolving this wide range of scales in a single fine-grained Large Eddy Simulation (LES) model would still be unfeasible due to its computational cost in terms of cell count and time stepping. Even the use of local mesh refinement to tackle the cell count problem would still require a very small time step to keep the Courant number below unity. Therefore, a nesting procedure is proposed to solve the both issues. An LES-within-LES nesting is composed of a Small-domain fine-grained LES (referred as S-LES from now), which is embedded in a Large-domain coarse-grained LES (referred as L-LES). The fields of the L-LES are interpolated on the boundaries of the S-LES to achieve the nesting. A blending zone, also named relaxation zone, is sometime added in the S-LES domain to ensure a smooth transition between the flow fields of the two simulations.

Reynolds Averaged Navier-Stokes (RANS) nesting procedures are already common practice for operational Numerical Weather Prediction (NWP). For example, most of the European meteorological offices use the a global planetary model to get macroscale climate prediction and transfer the relevant data to a nested NWP model for the mesoscale weather prediction.

The reference LES and coarse LES solve the standard filtered Navier-stokes equation for mass and momentum (Smagorinsky, 1963), which can be written in conservative form as:

$$\frac{\partial \overline{u}_i}{\partial x_i} = 0 \tag{2.1a}$$

$$\frac{\partial \overline{u}_i}{\partial t} + \frac{\partial \overline{u}_i \overline{u}_j}{\partial x_j} = -\frac{\partial \overline{p}}{\partial x_i} + \nu \frac{\partial^2 \overline{u}_i}{\partial x_j x_j} - \frac{\partial \tau_{ij}}{\partial x_j} \tag{2.1b}$$

with $\overline{p}$ and $\overline{u}_i$ the filtered (resolved) pressure and velocity fields, defined as

$$\overline{p} = p - p' \tag{2.2a}$$

$$\overline{u}_i = u_i - u_i' \tag{2.2b}$$

with p' and u_i' the residual pressure and velocity fields. On each filtered field, an averaging operation can be applied:

$$\langle \overline{p} \rangle = \overline{p} - p'' \tag{2.3a}$$

$$\langle \overline{u}_i \rangle = \overline{u}_i - u_i'' \tag{2.3b}$$

with $\langle \cdot \rangle$ the averaging operation on $\overline{p}$ and $\overline{u}_i$ fields, and p'', u_i'' the pressure and velocity fluctuation respectively.

The residual stress tensor τ_{ij}^{sgs}, also know as the sub-grid stress (sgs) tensor is defined as

$$\tau_{ij}^{sgs} = \overline{u_i u_j} - \overline{u}_i \overline{u}_j. \tag{2.4}$$

In this study the dynamic Smagorinsky-Lilly model proposed by Lilly, 1992 is used to modeled the sgs stress tensor. It is approximated by

$$\tau_{ij} = \frac{1}{3} \delta_{ij} \tau_{kk} + 2(C_D \Delta)^2 \left| \overline{S} \right| \overline{S}_{ij} \tag{2.5}$$

where $\delta_{ij} = 1$ if $i = j$ and zero otherwise, C_D the Smagorinsky co-efficient, Δ the filter size, and $\left| \overline{S} \right| = (2\overline{S}_{ij}\overline{S}_{ij})^2$ the magnitude of the stain-rate tensor $\overline{S}_{ij} = \left(\partial \overline{u}_i / \partial x_j + \partial \overline{u}_j / \partial x_i \right)/2$. In the original model, C_D is set as constant, which is not true near the wall and in the flow regions with high shear stresses. Therefore Lilly proposed a dynamic version of the C_D coefficient

$$C_D = \frac{1}{2} \frac{L_{ij} M_{ij}}{M_{ij}^2} \tag{2.6}$$

with

$$L_{ij} - \frac{1}{3}\delta_{ij}L_{kk} = 2C_D M_{ij} \tag{2.7a}$$

$$M_{ij} = \Delta^2 \left| \overline{S} \right| \overline{S}_{ij} - \Delta^2 \overline{\left| \overline{S} \right| \overline{S}_{ij}} \tag{2.7b}$$

which allows realistic values of C_D for wall bounded flow.

In the rest of this paper, the superscript $\cdot^R$ is used to describe any fields of the REF-LES. In a similar fashion, the superscripts $\cdot^L$ and $\cdot^S$ are used for L-LES and S-LES fields respectively.

The S-LES solves a modified set of filtered Navier-Stokes equations, which includes the implicit blending between the coarse-grained $\overline{u}_i^L$ and the fine-grained $\overline{u}_i^S$ velocity field. The mass and momentum conservation equations become

$$\frac{\partial \overline{u}_i^S}{\partial x_i} = 0 \tag{2.8a}$$

$$\frac{\partial \overline{u}_i^S}{\partial t} + \frac{\partial \overline{u}_i^S \overline{u}_j^S}{\partial x_j} = -\frac{\partial \overline{p}^S}{\partial x_i} + \nu \frac{\partial^2 \overline{u}_i^S}{\partial x_j x_j} - \frac{\partial \tau_{ij}^S}{\partial x_j} + \frac{w}{\tau_r}\left(\overline{u}_i^L - \overline{u}_i^S\right) \tag{2.8b}$$

with $w \in [0,1]$ the blending factor and τ_r the relaxation time. The fourth rhs term acts as a source term and enforces the blending. It acts by correcting the error between the calculated field $\overline{u}_i^S$ and the target field $\overline{u}_i^S$. Higher is the error, stronger is the correction.

2.2 LARGE EDDY SIMULATION

2.2.1 *Filtering operation*

2.2.1.1 *filtering the physical space*

2.2.1.2 *filtering the wavenumber space*

2.2.1.3 *filter width*

2.2.2 *Subgrid stress*

2.3 TURBULENCE MODELING IN LES

DISCUSSION

3.1 FIGURES AND IMAGES

The pillars of the creation taken by the Hubble Space Telescope on fig.3.1.

Figure 3.1: The pillars of the creation.

3.1.1 *Figures and Images in subsection*

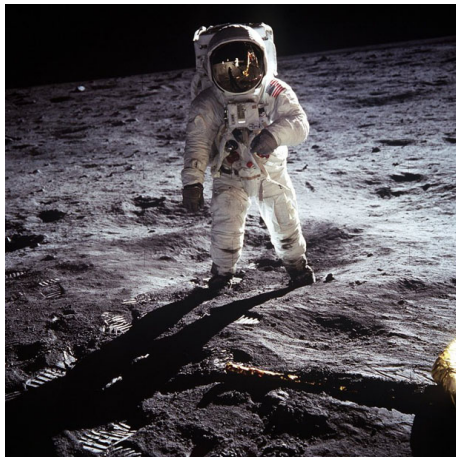On fig.3.2, a view of Buzz Aldrin on the moon.

Figure 3.2: Buzz Aldrin on the moon.

BIBLIOGRAPHY

Lilly, D. K. (1992). "A proposed modification of the Germano subgrid-scale closure method." In: *Physics of Fluids A: Fluid Dynamics* 4.3, p. 633. ISSN: 08998213. DOI: 10.1063/1.858280. URL: http://scitation.aip.org/content/aip/journal/pofa/4/3/10.1063/1.858280.

Moeng, C-H. et al. (2007). "Examining Two-Way Grid Nesting for Large Eddy Simulation of the PBL Using the WRF Model." In: *Monthly Weather Review* 135.6, pp. 2295–2311. ISSN: 0027-0644. DOI: 10.1175/MWR3406.1. URL: http://journals.ametsoc.org/doi/abs/10.1175/MWR3406.1.

Pope, Stephen (2000). *Turbulent Flows*. Cambridge University Press, p. 773. ISBN: 978-0-521-59886-6. URL: www.cambridge.org/9780521598866.

Smagorinsky, J. (1963). "General circulation experiments wiht the primitive equations I. The basic experiment." In: *Monthly Weather Review* 91.3, pp. 99–164. ISSN: 0036-8075. DOI: 10.1126/science.27.693.594.

NOTATION

PROBABILITY

SYMBOL	MEANING
$P(\cdot)$	probability mass function
Z	partition sum; normalization constant of a distribution
A	logarithm of the partition sum
A^*	conjugate dual of the log partition sum
$\mathbb{E}_P[X]$	expected value of X, w.r.t. distribution P
$\text{Cov}_P[X]$	covariance of X, w.r.t. distribution P
$D_{KL}(q\|p)$	Kullback-Leibler divergence of distributions q and p
$I(p,q)$	mutual information of p and q
$H(P)$	entropy of the distribution P
β	inverse temperature in a Gibbs distribution
$\mathbb{I}_{\text{expr}}(x)$	indicator function returning 1 if the Boolean expression expr involving variable x is true and 0 otherwise.

STRUCTURED OUTPUT

SYMBOL	MEANING
$\mathcal{Y}_i$	domain of the i-th output variable
y_i	individual output variable, $y_i \in \mathcal{Y}_i$
$\mathcal{Y}$	product space of all the individual output domains
$\boldsymbol{y}$	all the output variables of an example
$\mathcal{X}$	domain of the input variables
$\boldsymbol{x}$	all the input variables of an example
$\mathcal{Z}_i$	domain of the i-th hidden output variable
z_i	individual hidden output variable, $z_i \in \mathcal{Z}_i$
$\mathcal{Z}$	product space of all individual hidden output domains
$\boldsymbol{z}$	all the hidden output variables of an example
$\phi(\boldsymbol{x}, \boldsymbol{y})$	feature map of an example $(\boldsymbol{x}, \boldsymbol{y})$
$\psi(\boldsymbol{y}'|\boldsymbol{x}, \boldsymbol{y})$	feature map difference: $\phi(\boldsymbol{x}, \boldsymbol{y}') - \phi(\boldsymbol{x}, \boldsymbol{y})$
$\Delta_{\boldsymbol{y}^*}(\boldsymbol{y})$	loss when predicting $\boldsymbol{y}$ instead of $\boldsymbol{y}^*$
$\boldsymbol{w}$	(linear) parameters of a structured model
$\ell(\boldsymbol{w}, \boldsymbol{x}, \boldsymbol{y})$	surrogate loss of parameter $\boldsymbol{w}$ for example $(\boldsymbol{x}, \boldsymbol{y})$

FACTOR GRAPHS AND GRAPHICAL MODELS

SYMBOL	MEANING
$E(\boldsymbol{y})$	energy of output configuration $\boldsymbol{y}$
$\theta_c(\boldsymbol{y}_c)$	potential of factor c and assignment $\boldsymbol{y}_c$
$\bar{\theta}_c(\boldsymbol{y}_c)$	negative potential (score) of factor c and assignment $\boldsymbol{y}_c$
$\mathcal{G}$	graph
$\mathcal{V}$	vertices of a graph
$\mathcal{E}$	edges of a graph
$\mathcal{N}(i)$	neighboring vertices of vertex i
d_i	degree of the i-th vertex
$\mathcal{FG}$	factor graph
$\boldsymbol{\mu}$	marginal variables
$\mathcal{M}$	marginal polytope
$\mathcal{L}_{\mathcal{G}}$	local marginal polytope for graph $\mathcal{G}$

ACRONYMS

MAP	Maximum-A-Posteriori
MPE	Most Probable Explanation
MMSE	Minimum Mean Squared Error
MPM	Maximum Posteriori Marginal
ERM	Empirical Risk Minimization
MRF	Markov Random Field
CRF	Conditional Random Field
HCRF	Hidden Conditional Random Field
SVM	Support Vector Machine
mi-SVM	microscopic Multiple-Instance SVM
MI-SVM	macroscopic Multiple-Instance SVM
LP	Linear Program
QP	Quadratic Program
L-BFGS	limited-memory Broyden-Fletcher-Goldfarb-Shanno
OWL-QN	Orthant-Wise Limited-memory Quasi-Newton
SGD	Stochastic Gradient Descent
FISTA	Fast Iterative Shrinkage-Thresholding
ADMM	Alternating Direction Method of Multipliers
CCCP	Concave-Convex Procedure
DC	Difference of convex functions
SA	Simulated Annealing

MCMC	Markov Chain Monte Carlo
CD	Contrastive Divergence
KL	Kullback-Leibler
BP	Belief Propagation
MPLP	Max-Product Linear Programming
TRWS	Sequential Tree-Reweighted Message Passing
LPQP	Linear and Quadratic Program relaxation
LPQP-U	LPQP with Uniform Penalty
LPQP-T	LPQP with Tree-weighted Penalty
IBFS	Incremental Breadth First Search
FVS	Feedback Vertex Set
HOG	Histogram of Oriented Gradients
SIFT	Scale-invariant feature transform
OCR	Optical Character Recognition
VOC	Visual Object Classes

INDEX

CURRICULUM VITAE